

Light scattering by a vacuum-like sphere with magnetoelectric gyrotropy

A. D. Ulfat Jafri^a and Akhlesh Lakhtakia^{b,*}

^aDepartment of Electronics, Quaid-i-Azam University, Islamabad, Pakistan

^bNanoMM—Nanoengineered Metamaterials Group, Department of Engineering Science and Mechanics, Pennsylvania State University, University Park, PA 16802, USA

*Corresponding author: akhlesh@psu.edu

Abstract

An exact transition matrix was formulated for electromagnetic scattering by a vacuum-like sphere with magnetoelectric gyrotropy. Both the total scattering and forward scattering efficiencies are lower when the magnetoelectric gyrotropy vector of the sphere is co/anti-parallel to the electric field or magnetic field of an incident plane wave than when the magnetoelectric gyrotropy vector is coparallel to the propagation vector of the incident plane wave. Backscattering is absent when the propagation vector is co/anti-parallel to the magnetoelectric gyrotropy vector.

1 Introduction

The introduction of research on metamaterials has fuelled hope that the propagation of light in certain gravitational scenarios can be emulated in the laboratory [1, 2, 3, 4, 5], possibly as composite materials [6, 7]. The theoretical basis for this hope lies in the identification [8, 9] of the components of the gravitational metric $g_{\alpha\beta}$, $\alpha \in \{0, 1, 2, 3\}$ and $\beta \in \{0, 1, 2, 3\}$, with the components of the constitutive dyadics $\underline{\underline{\gamma}}$ and $\underline{\underline{\Gamma}} \times \underline{\underline{I}}$ of a linear bianisotropic continuum specified as

$$\left. \begin{aligned} \mathbf{D} &= \epsilon_0 \underline{\underline{\gamma}} \cdot \mathbf{E} - c_0^{-1} (\underline{\underline{\Gamma}} \times \underline{\underline{I}}) \cdot \mathbf{H} \\ \mathbf{B} &= \mu_0 \underline{\underline{\gamma}} \cdot \mathbf{H} + c_0^{-1} (\underline{\underline{\Gamma}} \times \underline{\underline{I}}) \cdot \mathbf{E} \end{aligned} \right\}, \quad (1)$$

where $\underline{\underline{I}}$ is the identity dyadic; ϵ_0 and μ_0 are the permittivity and the permeability of free space, respectively; and $c_0 = 1/\sqrt{\epsilon_0\mu_0}$. Specifically, when the metric $g_{\alpha\beta}$ has $(+, -, -, -)$ as its signature and \bar{g} denotes the determinant of $g_{\alpha\beta}$, we get $\gamma_{\ell m} = -(-\bar{g})^{1/2} g^{\ell m}/g_{00}$ and $\Gamma_\ell = g_{0\ell}/g_{00}$, $\ell \in \{1, 2, 3\}$ and $m \in \{1, 2, 3\}$. Thus, bianisotropic electromagnetics [10, 11] is already a theoretical testbed for gravitational research.

Free space, i.e., gravitationally unaffected vacuum, is the reference medium in electromagnetics [12]. A metric with $g_{0\ell} = 0 \forall \ell \in \{1, 2, 3\}$ identifies the 0th coordinate as time and delinks it from the remaining three coordinates (space); hence, the equivalent bianisotropic continuum is an anisotropic dielectric–magnetic which is devoid of magnetoelectric properties (i.e., $\underline{\underline{\Gamma}} = \mathbf{0}$) and is impedance-matched to free space. What would happen if a metric were such that its equivalent bianisotropic continuum is free space endowed with magnetoelectric gyrotropy (i.e., $\underline{\underline{\Gamma}} \neq \mathbf{0}$)? This communication arose from an attempt to answer that question.

Let u and $w_{1,2,3}$ be four real scalars of which only u is constrained to be non-zero and positive. Let these four scalars be used to construct the metric

$$[g_{\alpha\beta}] = u^{-1} (u + w_1^2 + w_2^2 + w_3^2)^{-1/4} \begin{bmatrix} 1 & w_1 & w_2 & w_3 \\ w_1 & -u & 0 & 0 \\ w_2 & 0 & -u & 0 \\ w_3 & 0 & 0 & -u \end{bmatrix}. \quad (2)$$

Then, $\bar{g}u^2 = -1$ and Eqs. (1) turn out to be

$$\left. \begin{aligned} \mathbf{D} &= \epsilon_0 \mathbf{E} - c_0^{-1} (\mathbf{w} \times \underline{\underline{I}}) \cdot \mathbf{H} \\ \mathbf{B} &= \mu_0 \mathbf{H} + c_0^{-1} (\mathbf{w} \times \underline{\underline{I}}) \cdot \mathbf{E} \end{aligned} \right\}, \quad (3)$$

where the magnetoelectric gyrotropy vector $\mathbf{w} = w_1 \hat{\mathbf{x}} + w_2 \hat{\mathbf{y}} + w_3 \hat{\mathbf{z}}$ in the Cartesian coordinate system. Clearly, the bianisotropic continuum equivalent to the metric (2) is like free space with magnetoelectric properties.

If an object made of a linear homogeneous material described by Eqs. (3) were to be placed in conventional free space, its scattering characteristics should depend on the magnitude and direction of \mathbf{w} . We decided to theoretically examine this proposition by considering the scattering of light by a sphere made of this material. For that purpose, we employed a recently formulated analytic procedure that relies on closed-form vector spherical wavefunctions for an orthorhombic dielectric-magnetic material with magnetoelectric gyrotropy [13]. In this procedure, a transition matrix (commonly called the ‘‘T matrix’’) describes scattering by the homogeneous sphere made of the chosen material.

The derivation of the T matrix for general nonspherical scatterers being available [13], we provide essential expressions and final results in Sec. 2. Section 3 presents numerical results to explicate the effects of magnetoelectric gyrotropy on the scattering of an incident plane wave. Special attention is paid to total scattering efficiency, the forward scattering efficiency, and the backscattering efficiency as functions of (i) the size parameter of the sphere and (ii) the magnitude and direction of \mathbf{w} in relation to the incident plane wave. The dependency $\exp(-i\omega t)$ on time t is present but suppressed, $k_0 = \omega/c_0$ is the free-space wave number, and $\eta_0 = \sqrt{\mu_0/\epsilon_0}$ is the intrinsic impedance of free space. The asterisk denotes the complex conjugate.

2 Theory

Suppose that the center of a homogeneous sphere of radius a and made of a material with constitutive relations (3) is located at the origin of a Cartesian coordinate system (x, y, z) . The ambient medium is free space. The sphere is illuminated by a plane wave with field phasors

$$\left. \begin{aligned} \mathbf{E}_{\text{inc}}(\mathbf{r}) &= \mathbf{e}_{\text{inc}} \exp(i\mathbf{k}_{\text{inc}} \cdot \mathbf{r}) \\ \mathbf{H}_{\text{inc}}(\mathbf{r}) &= \mathbf{h}_{\text{inc}} \exp(i\mathbf{k}_{\text{inc}} \cdot \mathbf{r}) \end{aligned} \right\}. \quad (4)$$

Without any loss of generality, we fix $\mathbf{k}_{\text{inc}} = k_0 \hat{\mathbf{z}}$, $\mathbf{e}_{\text{inc}} \parallel \hat{\mathbf{x}}$, and $\mathbf{h}_{\text{inc}} = (\omega\mu_0)^{-1} (\mathbf{k}_{\text{inc}} \times \mathbf{e}_{\text{inc}}) \parallel \hat{\mathbf{y}}$.

2.1 Incident-field representation

In order to formulate the T matrix, we must represent the incident field phasors (4) in terms of the vector spherical wavefunctions defined for free space as [14]

$$\left. \begin{aligned} \mathbf{M}_{emn}^{(1)}(k_0\mathbf{r}) &= \nabla \times [\mathbf{r}j_n(k_0r)P_n^m(\cos\theta)\cos(m\phi)] \\ \mathbf{M}_{omn}^{(1)}(k_0\mathbf{r}) &= \nabla \times [\mathbf{r}j_n(k_0r)P_n^m(\cos\theta)\sin(m\phi)] \\ \mathbf{N}_{smn}^{(1)}(k_0\mathbf{r}) &= k_0^{-1}\nabla \times \mathbf{M}_{smn}^{(1)}(k_0\mathbf{r}), \quad s \in \{e, o\} \end{aligned} \right\}, \quad (5)$$

$$m \in \{0, 1, 2, \dots, n\}, \quad n \in \{1, 2, 3, \dots\},$$

with $j_n(\cdot)$ denoting the spherical Bessel function of order n , and $P_n^m(\cdot)$ the associated Legendre function of order n and degree m . The spherical coordinate system (r, θ, ϕ) is equivalent to the Cartesian coordinate system (x, y, z) . The expansions [14, 15]

$$\mathbf{E}_{\text{inc}}(\mathbf{r}) = \sum_{n=1}^{\infty} \left\{ i^n \frac{2n+1}{n(n+1)} \left[\mathbf{M}_{o1n}^{(1)}(k_0\mathbf{r}) - i\mathbf{N}_{e1n}^{(1)}(k_0\mathbf{r}) \right] \right\}, \quad (6)$$

$$\mathbf{H}_{\text{inc}}(\mathbf{r}) = \frac{1}{i\eta_0} \sum_{n=1}^{\infty} \left\{ i^n \frac{2n+1}{n(n+1)} \left[\mathbf{N}_{o1n}^{(1)}(k_0\mathbf{r}) - i\mathbf{M}_{e1n}^{(1)}(k_0\mathbf{r}) \right] \right\}, \quad (7)$$

follow from Eqs. (4).

However, as the scattering sphere is made of a bianisotropic material, it is convenient to recast Eqs. (6) and (7) more generally as [13]

$$\mathbf{E}_{\text{inc}}(\mathbf{r}) = \sum_{s \in \{e,o\}} \sum_{n=1}^{\infty} \sum_{m=0}^n \left\{ D_{mn} \left[A_{smn}^{(1)} \mathbf{M}_{smn}^{(1)}(k_0 \mathbf{r}) + B_{smn}^{(1)} \mathbf{N}_{smn}^{(1)}(k_0 \mathbf{r}) \right] \right\}, \quad (8)$$

$$\mathbf{H}_{\text{inc}}(\mathbf{r}) = \frac{1}{i\eta_0} \sum_{s \in \{e,o\}} \sum_{n=1}^{\infty} \sum_{m=0}^n \left\{ D_{mn} \left[A_{smn}^{(1)} \mathbf{N}_{smn}^{(1)}(k_0 \mathbf{r}) + B_{smn}^{(1)} \mathbf{M}_{smn}^{(1)}(k_0 \mathbf{r}) \right] \right\}, \quad (9)$$

where the normalization factor

$$D_{mn} = (2 - \delta_{m0}) \frac{(2n+1)(n-m)!}{4n(n+1)(n+m)!} \quad (10)$$

employs the Kronecker delta δ_{mn} , and the coefficients

$$\left. \begin{aligned} A_{smn}^{(1)} &= i^n \frac{2n+1}{D_{mn}n(n+1)} \delta_{m1} \delta_{so}, \\ B_{smn}^{(1)} &= -i^{n+1} \frac{2n+1}{D_{mn}n(n+1)} \delta_{m1} \delta_{se} \end{aligned} \right\}. \quad (11)$$

2.2 Scattered-field representation

The scattered electric and magnetic field phasors are represented as [13]

$$\mathbf{E}_{\text{sca}}(\mathbf{r}) = \sum_{s \in \{e,o\}} \sum_{n=1}^{\infty} \sum_{m=0}^n \left\{ D_{mn} \left[A_{smn}^{(3)} \mathbf{M}_{smn}^{(3)}(k_0 \mathbf{r}) + B_{smn}^{(3)} \mathbf{N}_{smn}^{(3)}(k_0 \mathbf{r}) \right] \right\}, \quad r \geq a, \quad (12)$$

$$\mathbf{H}_{\text{sca}}(\mathbf{r}) = \frac{1}{i\eta_0} \sum_{s \in \{e,o\}} \sum_{n=1}^{\infty} \sum_{m=0}^n \left\{ D_{mn} \left[A_{smn}^{(1)} \mathbf{N}_{smn}^{(3)}(k_0 \mathbf{r}) + B_{smn}^{(3)} \mathbf{M}_{smn}^{(3)}(k_0 \mathbf{r}) \right] \right\}, \quad r \geq a. \quad (13)$$

In these expressions, the vectors spherical wavefunctions $\mathbf{M}_{smn}^{(3)}(k_0 \mathbf{r})$ and $\mathbf{N}_{smn}^{(3)}(k_0 \mathbf{r})$, respectively, are defined the same way as $\mathbf{M}_{smn}^{(1)}(k_0 \mathbf{r})$ and $\mathbf{N}_{smn}^{(1)}(k_0 \mathbf{r})$, except that the spherical Bessel function $j_n(\cdot)$ is replaced by the spherical Hankel function $h_n^{(1)}(\cdot)$ of the first kind [14]. The coefficients $A_{smn}^{(3)}$ and $B_{smn}^{(3)}$ have to be determined by the solution of a boundary-value problem [13].

In the far zone, the scattered electric field may be approximated as

$$\mathbf{E}_{\text{sca}}(\mathbf{r}) \approx \mathbf{F}_{\text{sca}}(\theta, \phi) \frac{\exp(ik_0 r)}{r} \quad (14)$$

and the scattered magnetic field as

$$\mathbf{H}_{\text{sca}}(\mathbf{r}) \approx \eta_0^{-1} \hat{\mathbf{r}} \times \mathbf{F}_{\text{sca}}(\theta, \phi) \frac{\exp(ik_0 r)}{r}, \quad (15)$$

where $\hat{\mathbf{r}} = \mathbf{r}/r$ and $\mathbf{F}_{\text{sca}}(\theta, \phi)$ is the vector far-field scattering amplitude [16]. The differential scattering efficiency is given by

$$Q_D(\theta, \phi) = \frac{4}{a^2} \frac{\mathbf{F}_{\text{sca}}(\theta, \phi) \cdot \mathbf{F}_{\text{sca}}^*(\theta, \phi)}{\mathbf{e}_{\text{inc}} \cdot \mathbf{e}_{\text{inc}}^*}. \quad (16)$$

and total scattering efficiency is given as

$$\sigma_{\text{sca}} = \frac{1}{\mathbf{e}_{\text{inc}} \cdot \mathbf{e}_{\text{inc}}^*} \int_{\phi=0}^{2\pi} \int_{\theta=0}^{\pi} [\mathbf{F}_{\text{sca}}(\theta, \phi) \cdot \mathbf{F}_{\text{sca}}^*(\theta, \phi)] \sin \theta \, d\theta \, d\phi \quad (17)$$

$$Q_{\text{sca}} = \frac{1}{\mathbf{e}_{\text{inc}} \cdot \mathbf{e}_{\text{inc}}^*} \frac{1}{(k_0 a)^2} \sum_{s \in \{e, o\}} \sum_{n=1}^{\infty} \sum_{m=0}^n \left[D_{mn} \left(|A_{smn}^{(3)}|^2 + |B_{smn}^{(3)}|^2 \right) \right]. \quad (18)$$

2.3 Internal-field representation

The electric and magnetic field phasors excited inside the vacuum-like sphere with magnetoelectric gyrotropy are represented by [13, 17]

$$\begin{aligned} \mathbf{E}_{\text{exc}}(\mathbf{r}) = \exp(ik_0 \mathbf{w} \cdot \mathbf{r}) \sum_{s \in \{e, o\}} \sum_{n=1}^{\infty} \sum_{m=0}^n \left[b_{smn} \mathbf{M}_{smn}^{(1)}(k_0 \mathbf{r}) \right. \\ \left. + c_{smn} \mathbf{N}_{smn}^{(1)}(k_0 \mathbf{r}) \right], \quad r \leq a, \end{aligned} \quad (19)$$

$$\begin{aligned} \mathbf{H}_{\text{exc}}(\mathbf{r}) = \frac{1}{i\eta_0} \exp(ik_0 \mathbf{w} \cdot \mathbf{r}) \sum_{s \in \{e, o\}} \sum_{n=1}^{\infty} \sum_{m=0}^n \left[b_{smn} \mathbf{N}_{smn}^{(1)}(k_0 \mathbf{r}) \right. \\ \left. + c_{smn} \mathbf{M}_{smn}^{(1)}(k_0 \mathbf{r}) \right], \quad r \leq a, \end{aligned} \quad (20)$$

the coefficients b_{smn} and c_{smn} being unknown.

2.4 Solution of boundary-value problem

The standard boundary conditions

$$\left. \begin{aligned} \hat{\mathbf{r}} \times \mathbf{E}_{\text{exc}}(\mathbf{r}) &= \hat{\mathbf{r}} \times [\mathbf{E}_{\text{inc}}(\mathbf{r}) + \mathbf{E}_{\text{sca}}(\mathbf{r})] \\ \hat{\mathbf{r}} \times \mathbf{H}_{\text{exc}}(\mathbf{r}) &= \hat{\mathbf{r}} \times [\mathbf{H}_{\text{inc}}(\mathbf{r}) + \mathbf{H}_{\text{sca}}(\mathbf{r})] \end{aligned} \right\}, \quad r = a, \quad (21)$$

hold across the surface of the sphere. Their application yields the following set of algebraic equations for every combination of $j \in \{1, 3\}$, $s \in \{e, o\}$, $n \in \{1, 2, 3, \dots\}$, and $m \in \{0, 1, 2, \dots, n\}$ [13]:

$$A_{smn}^{(1)} = \sum_{s' \in \{e, o\}} \sum_{n'=1}^{\infty} \sum_{m'=0}^{n'} \left[I_{smn, s' m' n'}^{(1)} b_{s' m' n'} + J_{smn, s' m' n'}^{(1)} c_{s' m' n'} \right], \quad (22)$$

$$B_{smn}^{(1)} = \sum_{s' \in \{e, o\}} \sum_{n'=1}^{\infty} \sum_{m'=0}^{n'} \left[J_{smn, s' m' n'}^{(1)} b_{s' m' n'} + I_{smn, s' m' n'}^{(1)} c_{s' m' n'} \right], \quad (23)$$

$$A_{smn}^{(3)} = - \sum_{s' \in \{e, o\}} \sum_{n'=1}^{\infty} \sum_{m'=0}^{n'} \left[I_{smn, s' m' n'}^{(3)} b_{s' m' n'} + J_{smn, s' m' n'}^{(3)} c_{s' m' n'} \right], \quad (24)$$

$$B_{smn}^{(3)} = - \sum_{s' \in \{e, o\}} \sum_{n'=1}^{\infty} \sum_{m'=0}^{n'} \left[J_{smn, s' m' n'}^{(3)} b_{s' m' n'} + I_{smn, s' m' n'}^{(3)} c_{s' m' n'} \right]. \quad (25)$$

In these equations, the quantities $I_{smn, s' m' n'}^{(j)}$ and $J_{smn, s' m' n'}^{(j)}$ are computed as surface integrals. Thus,

$$\begin{aligned} I_{smn, s' m' n'}^{(j)} = \frac{i(k_0 a)^2}{\pi} \int_0^{2\pi} d\phi \int_0^{\pi} d\theta \sin \theta \left\{ \hat{\mathbf{r}} \cdot \left[\mathbf{M}_{smn}^{(\ell)}(k_0 a \hat{\mathbf{r}}) \times \mathbf{N}_{s' m' n'}^{(1)}(k_0 a \hat{\mathbf{r}}) \right. \right. \\ \left. \left. + \mathbf{N}_{smn}^{(\ell)}(k_0 a \hat{\mathbf{r}}) \times \mathbf{M}_{s' m' n'}^{(1)}(k_0 a \hat{\mathbf{r}}) \right] \exp(ik_0 a \mathbf{w} \cdot \hat{\mathbf{r}}) \right\} \end{aligned} \quad (26)$$

and

$$J_{smn,s'm'n'}^{(j)} = \frac{i(k_0 a)^2}{\pi} \int_0^{2\pi} d\phi \int_0^\pi d\theta \sin\theta \left\{ \hat{\mathbf{r}} \cdot \left[\mathbf{M}_{smn}^{(\ell)}(k_0 a \hat{\mathbf{r}}) \times \mathbf{M}_{s'm'n'}^{(1)}(k_0 a \hat{\mathbf{r}}) + \mathbf{N}_{smn}^{(\ell)}(k_0 a \hat{\mathbf{r}}) \times \mathbf{N}_{s'm'n'}^{(1)}(k_0 a \hat{\mathbf{r}}) \right] \exp(ik_0 a \mathbf{w} \cdot \hat{\mathbf{r}}) \right\}, \quad (27)$$

where $j \in \{1, 3\}$, $\ell = j + 2 \pmod{4} \in \{3, 1\}$, and $\hat{\mathbf{r}} = (\hat{\mathbf{x}} \cos \phi + \hat{\mathbf{y}} \sin \phi) \sin \theta + \hat{\mathbf{z}} \cos \theta$ is the unit radial vector. The integrals over ϕ can be handled analytically, but it is more convenient to evaluate them numerically. The integrals over θ require numerical integration. Let us also note that $I_{smn,s'm'n'}^{(3)} = -I_{s'm'n',smn}^{(3)}$, $J_{smn,s'm'n'}^{(3)} = -J_{s'm'n',smn}^{(3)}$, and $I_{smn,smn}^{(3)} = J_{smn,smn}^{(3)} = 0$, but similar skew-symmetric features are not displayed, in general, by $I_{smn,s'm'n'}^{(1)}$ and $J_{smn,s'm'n'}^{(1)}$.

The summations over $n' \in \{1, 2, 3, \dots\}$ are restricted to $n' \in \{1, 2, 3, \dots, N\}$ and similarly $n \in \{1, 2, 3, \dots\}$ to $n \in \{1, 2, 3, \dots, N\}$. Then, Eqs. (22)–(25) can be written down symbolically in matrix form as

$$\begin{bmatrix} [A^{(1)}] \\ [B^{(1)}] \end{bmatrix} = \begin{bmatrix} [I^{(1)}] & [J^{(1)}] \\ [J^{(1)}] & [I^{(1)}] \end{bmatrix} \begin{bmatrix} [b] \\ [c] \end{bmatrix} \equiv [Y^{(1)}] \begin{bmatrix} [b] \\ [c] \end{bmatrix} \quad (28)$$

and

$$\begin{bmatrix} [A^{(3)}] \\ [B^{(3)}] \end{bmatrix} = - \begin{bmatrix} [I^{(3)}] & [J^{(3)}] \\ [J^{(3)}] & [I^{(3)}] \end{bmatrix} \begin{bmatrix} [b] \\ [c] \end{bmatrix} \equiv - [Y^{(3)}] \begin{bmatrix} [b] \\ [c] \end{bmatrix}. \quad (29)$$

Here, the column vectors $[A^{(j)}]$ and $[B^{(j)}]$ contain the coefficients $A_{smn}^{(j)}$ and $B_{smn}^{(j)}$, respectively, arranged in a specified order, with similar interpretations for the column vectors $[b]$ and $[c]$. Furthermore, $[I^{(j)}]$ and $[J^{(j)}]$ are matrixes in which the integrals $I_{smn,s'm'n'}^{(j)}$ and $J_{smn,s'm'n'}^{(j)}$, respectively, are arranged in consonance with the column vectors $[A^{(j)}]$, etc.

Equations (28) and (29) lead to the relation

$$\begin{bmatrix} [A^{(3)}] \\ [B^{(3)}] \end{bmatrix} = [T] \begin{bmatrix} [A^{(1)}] \\ [B^{(1)}] \end{bmatrix}, \quad (30)$$

wherein $[T] = - [Y^{(3)}] [Y^{(1)}]^{-1}$ is the T matrix of the chosen sphere suspended in free space. Because of the structure of the matrix $[Y^{(j)}]$, the T matrix can be partitioned as

$$[T] \equiv \begin{bmatrix} [T^{(A)}] & [T^{(AB)}] \\ [T^{(AB)}] & [T^{(B)}] \end{bmatrix}. \quad (31)$$

3 Numerical results and discussion

We set up a MathematicaTM program to compute the T matrix. In the program, we truncated the summations over $n' \in \{1, 2, 3, \dots\}$ to $n' \in \{1, 2, 3, \dots, N\}$ and similarly $n \in \{1, 2, 3, \dots\}$ to $n \in \{1, 2, 3, \dots, N\}$. We chose sufficiently high values of N , such that the extinction efficiency Q_{ext} , the total scattering efficiency Q_{sca} , the forward scattering efficiency Q_f , and the backscattering efficiency Q_b [16] converged to a pre-set tolerance of 0.1%. Smaller values of $|\mathbf{w}|$ and $k_0 a$ required smaller N , with $N = 11$ being adequate for $|\mathbf{w}| = 0.25$ and $k_0 a = 4.0$.

We confirmed that our program yielded negligibly tiny values of the coefficients $A_{smn}^{(3)}$ and $B_{smn}^{(3)}$ when we set $\mathbf{w} = \mathbf{0}$. When $\mathbf{w} \perp \hat{\mathbf{z}}$, reversal of the direction of \mathbf{w} was tantamount to the multiplication of $A_{smn}^{(3)}$, $B_{smn}^{(3)}$, b_{smn} , and c_{smn} by negative unity, which left Q_{ext} , Q_{sca} , Q_f , and Q_b unchanged. When $\mathbf{w} \parallel \hat{\mathbf{z}}$, both \mathbf{w} and the direction of propagation of the incident plane wave had to be reversed together for Q_{ext} , Q_{sca} , Q_f , and Q_b to remain unchanged. Regardless of the choice of \mathbf{w} , we found that $Q_{\text{ext}} = Q_{\text{sca}}$, implying that the absorption efficiency $Q_{\text{abs}} = 0$. This was expected because Eqs. (3) satisfy the conditions of the absence of dissipation [18, 11].

Although the magnetoelectric gyrotropy vector \mathbf{w} can be arbitrarily oriented, three cases are of particular interest because the incident light is a plane wave:

- \mathbf{w} is parallel to the incident electric field (i.e., $\mathbf{w} \parallel \hat{\mathbf{x}}$),
- \mathbf{w} is parallel to the incident magnetic field (i.e., $\mathbf{w} \parallel \hat{\mathbf{y}}$), and
- \mathbf{w} is parallel to the propagation vector of the incident plane wave (i.e., $\mathbf{w} \parallel \hat{\mathbf{z}}$).

3.1 Efficiencies

Figure 1 shows plots of Q_{sca} , Q_f , and Q_b as functions of the size parameter k_0a when $\mathbf{w} \parallel \mathbf{e}_{\text{inc}}$ and $|\mathbf{w}| \in \{0.05, 0.15, 0.25\}$. An increase in the magnitude of the magnetoelectric gyrotropy vector has a more pronounced effect on Q_f than on Q_{sca} and Q_b . Whereas Q_{sca} is higher than Q_f for smaller values of $|\mathbf{w}|$ and k_0a , the reverse is true for larger values of $|\mathbf{w}|$ and k_0a . The backscattering efficiency shows oscillatory behavior and peaks of the oscillations increase as the size parameter increases.

The plots of Q_{sca} , Q_f , and Q_b as functions of the size parameter k_0a when $\mathbf{w} \parallel \mathbf{h}_{\text{inc}}$ are identical to those when $\mathbf{w} \parallel \mathbf{e}_{\text{inc}}$. Thus, the effect of magnetoelectric gyrotropy is independent of its orientation when $\mathbf{w} \perp \mathbf{k}_{\text{inc}}$.

Figure 2 shows plots of Q_{sca} , Q_f , and Q_b as functions of the size parameter k_0a when $\mathbf{w} \parallel \mathbf{k}_{\text{inc}}$ and $|\mathbf{w}| \in \{0.05, 0.15, 0.25\}$. The influence of magnetoelectric gyrotropy is maximal when $\mathbf{w} \parallel \mathbf{k}_{\text{inc}}$, as is evident from a comparison of Figs. 1 and 2. The maximum value of Q_{sca} is an order of magnitude higher and Q_f in Fig. 1 is two orders of magnitude higher when $\mathbf{w} \parallel \mathbf{k}_{\text{inc}}$ than when $\mathbf{w} \perp \mathbf{k}_{\text{inc}}$. Moreover, there is no backscattering (i.e., $Q_b = 0$) when $\mathbf{w} \parallel \mathbf{k}_{\text{inc}}$, which makes the sphere invisible in the monostatic configuration.

The absence of backscattering when $\mathbf{w} \parallel \mathbf{k}_{\text{inc}}$ has an analog [19] in the reflection of a plane wave incident normally at the planar interface of free space and the material with constitutive relations (3) such that \mathbf{w} is oriented wholly normal to the interface. Simple algebraic manipulations show that reflection is then absent (and transmission is perfect).

Figure 3 shows the same plots as Fig. 2, except that $w_3 < 0$. A change in the sign of w_3 affects both Q_{sca} and Q_f , as is clear from comparing Figs. 2 and 3. Both Q_{sca} and Q_f are higher when \mathbf{w} is coparallel, than when \mathbf{w} is antiparallel, to the propagation vector \mathbf{k}_{inc} of the incident plane wave.

Given the foregoing trends, for arbitrarily directed \mathbf{w} it is reasonable to expect that the effects of the component of \mathbf{w} that is co/anti-parallel to the propagation vector of the incident plane wave would dominate those of the component of \mathbf{w} that is perpendicular to the propagation vector. Several calculations (not shown) validated that expectation.

3.2 Differential scattering efficiency

For $k_0a = 4$, $|\mathbf{w}| = 0.25$, and four different orientations of \mathbf{w} , the differential scattering efficiencies $Q_D(\theta, 0^\circ)$ and $Q_D(\theta, 90^\circ)$ are plotted versus the observation angle $\theta \in [0^\circ, 180^\circ]$ in Fig. 4. The curve of $Q_D(\theta, 0^\circ)$ when $\mathbf{w} \parallel \mathbf{e}_{\text{inc}}$ [Fig. 4(a)] is identical to that of $Q_D(\theta, 90^\circ)$ when $\mathbf{w} \parallel \mathbf{h}_{\text{inc}}$ [Fig. 4(b)]. Likewise, the curve of $Q_D(\theta, 90^\circ)$ for $\mathbf{w} \parallel \mathbf{e}_{\text{inc}}$ is identical to that of $Q_D(\theta, 0^\circ)$ for $\mathbf{w} \parallel \mathbf{h}_{\text{inc}}$. This shows that the impact of magnetoelectric gyrotropy is largely independent of its orientation when $\mathbf{w} \perp \mathbf{k}_{\text{inc}}$. More lobes appear in the curve of $Q_D(\theta, 0^\circ)$ as compared to $Q_D(\theta, 90^\circ)$, and the maximum magnitude of the former is smaller than that of the latter, when $\mathbf{w} \parallel \mathbf{e}_{\text{inc}}$.

When \mathbf{w} is co/anti-parallel to \mathbf{k}_{inc} , the differential scattering appears identical in the $\phi = 0^\circ$ and $\phi = 90^\circ$ planes, as shown in Figs. 4(c) and 4(d). However, more lobes exist when \mathbf{w} is co-parallel than when it is anti-parallel to \mathbf{k}_{inc} .

3.3 Rayleigh scattering

A long-wavelength approximation yields closed-form analytical results for scattering by homogeneous and electrically small objects [20]. Accordingly, Rayleigh scattering by the chosen sphere is equivalent to radiation

jointly by an electric dipole moment

$$\mathbf{p}_{\text{eqvt}} = - \left(\frac{4\pi a^3}{3} \right) \frac{\epsilon_0}{1 - (|\mathbf{w}|/3)^2} (\mathbf{w} \times \underline{\mathbf{I}}) \cdot \left[\left(\hat{\mathbf{k}}_{\text{inc}} \times \underline{\mathbf{I}} \right) - \frac{1}{3} (\mathbf{w} \times \underline{\mathbf{I}}) \right] \cdot \mathbf{e}_{\text{inc}} \quad (32)$$

and a magnetic dipole moment

$$\mathbf{m}_{\text{eqvt}} = \left(\frac{4\pi a^3}{3} \right) \frac{\sqrt{\mu_0 \epsilon_0}}{1 - (|\mathbf{w}|/3)^2} (\mathbf{w} \times \underline{\mathbf{I}}) \cdot \left[\underline{\mathbf{I}} + \frac{1}{3} (\mathbf{w} \times \underline{\mathbf{I}}) \cdot \left(\hat{\mathbf{k}}_{\text{inc}} \times \underline{\mathbf{I}} \right) \right] \cdot \mathbf{e}_{\text{inc}} \quad (33)$$

both located at the centroid of the sphere, with $\hat{\mathbf{k}}_{\text{inc}} = \mathbf{k}_{\text{inc}}/k_0$. Clearly from these expressions, both equivalent dipole moments vanish as $|\mathbf{w}| \rightarrow 0$.

Therefore, the Rayleigh estimate of the vector far-field scattering amplitude is [16, 20]

$$\mathbf{F}_{\text{sca}}^{\text{Rayleigh}}(\hat{\mathbf{r}}) = - \frac{\omega^2 \mu_0}{4\pi} \left[\hat{\mathbf{r}} \times (\hat{\mathbf{r}} \times \mathbf{p}_{\text{eqvt}}) + \eta_0^{-1} \hat{\mathbf{r}} \times \mathbf{m}_{\text{eqvt}} \right], \quad (34)$$

wherefrom the Rayleigh estimates of the various efficiencies were obtained as follows:

$$\begin{aligned} Q_{\text{sca}}^{\text{Rayleigh}} &= \frac{8(k_0 a)^4}{3(\mathbf{w} \cdot \mathbf{w} - 9)^2} \\ &\times \left[(w_1^2 + w_2^2)^2 + 3(w_1^2 + w_2^2)(w_3 - 1)(w_3 - 3) \right. \\ &\quad \left. + 2w_3^2(w_3 - 3)^2 \right], \end{aligned} \quad (35)$$

$$Q_f^{\text{Rayleigh}} = \frac{4(k_0 a)^4}{(\mathbf{w} \cdot \mathbf{w} - 9)^2} [w_1^2 + w_2^2 + 2w_3(w_3 - 3)]^2, \quad (36)$$

$$Q_b^{\text{Rayleigh}} = \frac{4(k_0 a)^4}{(\mathbf{w} \cdot \mathbf{w} - 9)^2} (w_1^2 + w_2^2)^2. \quad (37)$$

Neither w_1 nor w_2 occur by themselves in the foregoing expressions, but always as $w_1^2 + w_2^2$. Therefore, when $\mathbf{w} \perp \mathbf{k}_{\text{inc}}$, the three efficiencies

$$Q_{\text{sca}}^{\text{Rayleigh}} = \frac{8(k_0 a)^4}{3(\mathbf{w} \cdot \mathbf{w} - 9)^2} (\mathbf{w} \cdot \mathbf{w})(\mathbf{w} \cdot \mathbf{w} + 9), \quad (38)$$

$$Q_f^{\text{Rayleigh}} = Q_b^{\text{Rayleigh}} = \frac{4(k_0 a)^4}{(\mathbf{w} \cdot \mathbf{w} - 9)^2} (\mathbf{w} \cdot \mathbf{w})^2, \quad (39)$$

contain the quadratic form $\mathbf{w} \cdot \mathbf{w}$ and are invariant with respect to the orientation of the magnetoelectric gyrotropy vector.

In contrast when $\mathbf{w} \parallel \mathbf{k}_{\text{inc}}$, the efficiencies

$$Q_{\text{sca}}^{\text{Rayleigh}} = \frac{1}{3} Q_f^{\text{Rayleigh}} = \frac{16(k_0 a)^4 w^2}{3(w + 3)^2} \quad (40)$$

do depend on the orientation of the magnetoelectric gyrotropy vector. However, from Eq. (37) it follows that $Q_b^{\text{Rayleigh}} = 0$ does not.

The Rayleigh expressions are expected to hold when the radius of the sphere is less than a tenth of the free-space wavelength. As an example, Fig. 5 depicts plots of $Q_{\text{sca}}^{\text{Rayleigh}}$ and Q_b^{Rayleigh} versus $k_0 a \in (0, 0.6]$ for $|\mathbf{w}| = 0.25$. Clearly, the long-wavelength approximation agrees well for entire range of $k_0 a$ when \mathbf{w} is coparallel to \mathbf{k}_{inc} . When \mathbf{w} is parallel to the incident electric/magnetic field or \mathbf{w} is antiparallel to \mathbf{k}_{inc} , the results match well for $k_0 a \in (0, 0.4]$ but the difference between the exact and approximate results begins to rise as the value of $k_0 a$ increases beyond 0.4.

4 Concluding remarks

Electromagnetic scattering by a vacuum-like sphere with magnetoelectric gyrotropy was formulated in terms of the T matrix, after simplifying recently derived vector spherical wavefunctions in closed form. The total scattering, extinction, forward scattering, and backscattering efficiencies were computed to explicate the magnitude and the direction of the magnetoelectric gyrotropy vector in relation to the directions of the propagation vector, the magnetic field, and the electric field of a plane wave incident on the chosen sphere.

Since the permittivity and the permeability of the sphere are exactly the same as those of the surrounding vacuum, any scattering must be attributed solely to the magnetoelectric gyrotropy vector of the sphere. In general, all scattering efficiencies grow as the magnetoelectric gyrotropy grows in magnitude. A growing trend in all efficiencies with increase in the electrical size of the sphere was also found, though the growth may not be monotonic but undulatory.

Both the total scattering and forward scattering efficiencies are generally lower when the magnetoelectric gyrotropy vector of the sphere is perpendicular to the propagation vector of the incident plane wave than when it is anti-parallel to the propagation vector. Further enhancements occur when the magnetoelectric gyrotropy vector is co-parallel to the propagation vector. Furthermore, the sphere is invisible in monostatic configuration provided that the magnetoelectric gyrotropy vector is co/anti-parallel to the propagation vector.

Acknowledgments

A.D.U.J. thanks the Higher Education Commission of Pakistan and A.L. is grateful to the Charles Godfrey Binder Endowment at the Pennsylvania State University for supporting this research.

References

- [1] B. Chen and R. Kantowski, “Including absorption in Gordon’s optical metric,” *Phys. Rev. D* **79**, 104007 (2009).
- [2] T. G. Mackay and A. Lakhtakia, “Towards a metamaterial simulation of a spinning cosmic string,” *Phys. Lett. A* **374**, 2305–2308 (2010).
- [3] H. Chen, R.-X. Miao, and M. Li, “Transformation optics that mimics the system outside a Schwarzschild black hole,” *Opt. Express* **18**, 15183–15188 (2010).
- [4] A. I. Smolyaninov and I. I. Smolyaninov, “Lattice models of nontrivial ‘optical spaces’ based on metamaterial waveguides,” *Opt. Lett.* **36**, 2420–2422 (2011).
- [5] I. I. Smolyaninov and Y.-J. Hung, “Minkowski domain walls in hyperbolic metamaterials,” *Phys. Lett. A* **377**, 353–356 (2013).
- [6] W. Lu, J. Jin, Z. Lin, and H. Chen, “A simple design of an artificial electromagnetic black hole,” *J. Appl. Phys.* **108**, 064517 (2010).
- [7] T. G. Mackay and A. Lakhtakia, “Towards a realization of Schwarzschild-(anti-)de Sitter spacetime as a particulate metamaterial,” *Phys. Rev. B* **83**, 195424 (2011).
- [8] J. Plebanski, “Electromagnetic waves in gravitational fields,” *Phys. Rev.* **118**, 1396–1408 (1960).
- [9] T. G. Mackay, A. Lakhtakia, and S. Setiawan, “Gravitation and electromagnetic wave propagation with negative phase velocity,” *New J. Phys.* **7**, 75 (2005).
- [10] D. K. Cheng and J. A. Kong, “Covariant descriptions of bianisotropic media,” *Proc. IEEE* **56**, 248–251 (1968).

- [11] T. G. Mackay and A. Lakhtakia, *Electromagnetic Anisotropy and Bianisotropy: A Field Guide* (World Scientific, 2010), Chap. 1.
- [12] E. J. Post, *Formal Structure of Electromagnetics* (North-Holland, 1962).
- [13] A. Lakhtakia and T. G. Mackay, “Vector spherical wavefunctions for orthorhombic dielectric-magnetic material with gyrotropic-like magnetoelectric properties,” *J. Opt. (India)* **41**, 201–213 (2012).
- [14] J. A. Stratton, *Electromagnetic Theory* (McGraw–Hill, 1941), Chap. 7.
- [15] C. F. Bohren and D. R. Huffman, *Absorption and Scattering of Light by Small Particles* (Wiley, 1983), Chap. 4.
- [16] A. D. U. Jafri and A. Lakhtakia, “Scattering of an electromagnetic plane wave by a homogeneous sphere made of an orthorhombic dielectric-magnetic material,” *J. Opt. Soc. Am. A* **31**, 89–100 (2014). The negative sign (–) after the second equal sign (=) in Eq. (48) of this paper is a typographical error and must be removed.
- [17] A. Lakhtakia and W. S. Weiglhofer, “On electromagnetic fields in a linear medium with gyrotropic-like magnetoelectric properties,” *Microw. Opt. Technol. Lett.* **15**, 168–170 (1997).
- [18] B. D. H. Tellegen, “The gyrator, a new electric network element,” *Philips Res. Rep.* **3**, 81–101 (1948).
- [19] C. F. Bohren, “Scattering by a sphere and reflection by a slab: some notable similarities,” *Appl. Opt.* **27**, 205–206 (1988).
- [20] A. Lakhtakia, “Rayleigh scattering by a bianisotropic ellipsoid in a biisotropic medium,” *Int. J. Electron.* **71**, 1057–1062 (1991).

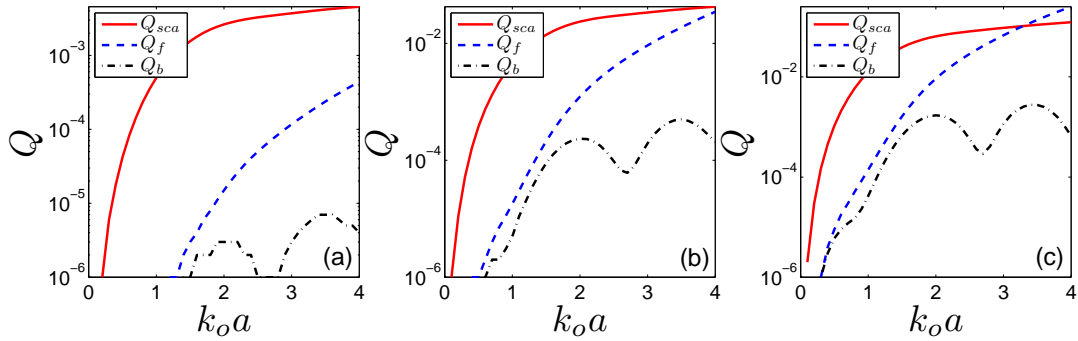


Figure 1: Q_{sca} , Q_f , and Q_b as functions of the size parameter $k_0 a$, when \mathbf{w} is parallel to the incident electric field; $w_2 = w_3 = 0$, but (a) $w_1 = 0.05$, (b) $w_1 = 0.15$, and (c) $w_1 = 0.25$. These plots also hold true when \mathbf{w} is parallel to the incident magnetic field; $w_1 = w_3 = 0$, but (a) $w_2 = 0.05$, (b) $w_2 = 0.15$, and (c) $w_2 = 0.25$.

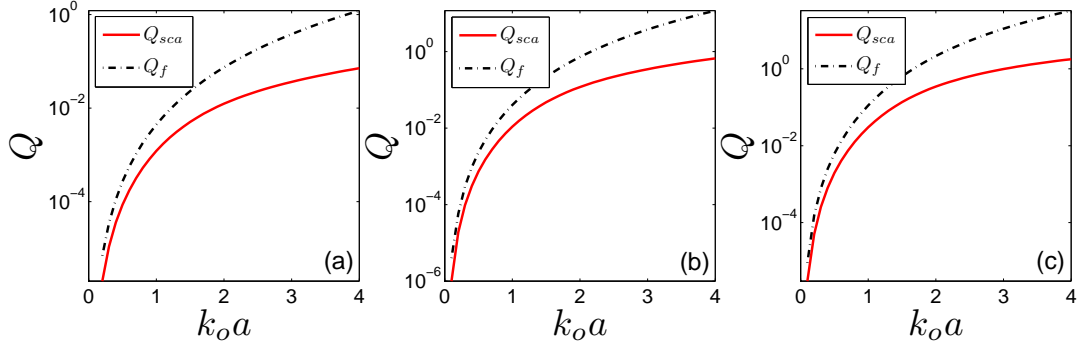


Figure 2: Q_{sca} and Q_f as functions of the size parameter $k_0 a$, when \mathbf{w} is parallel to the direction of propagation of the incident plane wave; $w_1 = w_2 = 0$, but (a) $w_3 = 0.05$, (b) $w_3 = 0.15$, and (c) $w_3 = 0.25$. $Q_b \equiv 0$ when $\mathbf{w} \parallel \mathbf{k}_{inc}$.

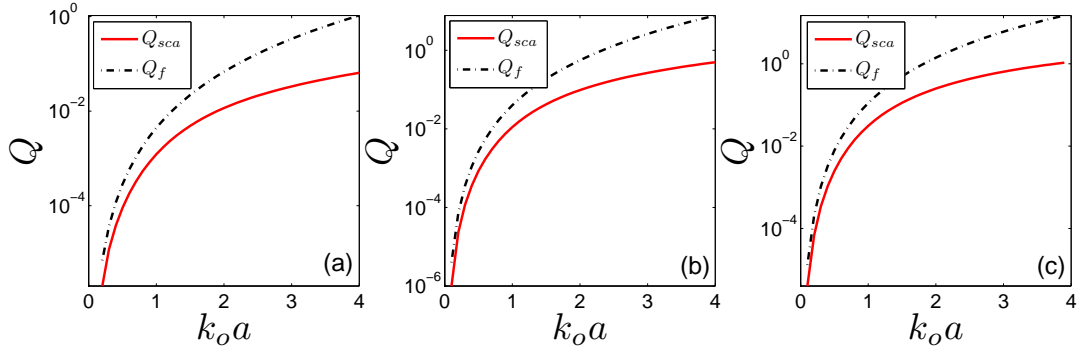


Figure 3: Same as Fig. 2, except that (a) $w_3 = -0.05$, (b) $w_3 = -0.15$, and (c) $w_3 = -0.25$.

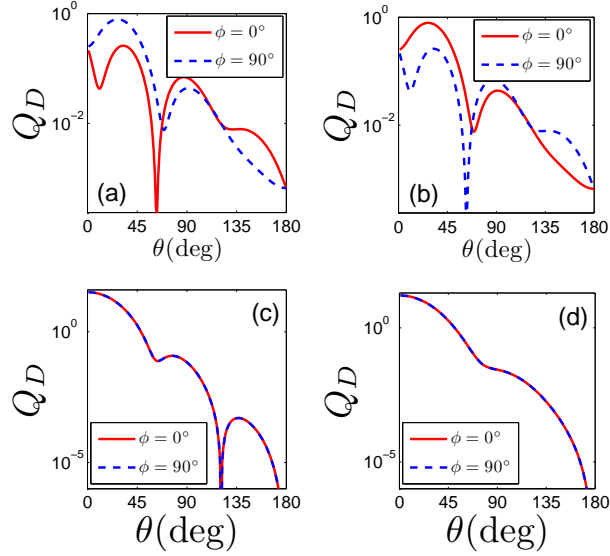


Figure 4: Q_D as a function of $\theta \in [0^\circ, 180^\circ]$ and $\phi = \{0^\circ, 90^\circ\}$ for $k_0 a = 4$, when (a) $w_1 = 0.25, w_2 = w_3 = 0$; (b) $w_1 = w_3 = 0, w_2 = 0.25$; (c) $w_1 = w_2 = 0, w_3 = 0.25$; and (d) $w_1 = w_2 = 0, w_3 = -0.25$.

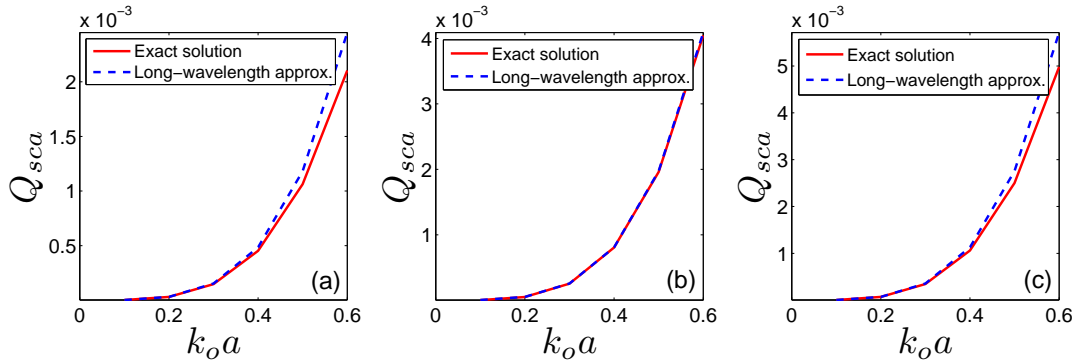


Figure 5: Total scattering efficiency computed exactly using Eq. (18) and approximately using Eq. (34) as a function of $k_0 a$ when (a) $w_2 = w_3 = 0, w_1 = 0.25$; (b) $w_1 = w_2 = 0, w_3 = 0.25$; and (c) $w_1 = w_2 = 0, w_3 = -0.25$.